

PAPER

Low temperature injected-caused charge carrier instability in n-type silicon below insulator-to-metal transition

To cite this article: A L Danilyuk *et al* 2020 *J. Phys.: Condens. Matter* **32** 225702

View the [article online](#) for updates and enhancements.




IOP | ebooks™

Bringing you innovative digital publishing with leading voices to create your essential collection of books in STEM research.

Start exploring the [collection](#) - download the first chapter of every title for free.

Low temperature injected-caused charge carrier instability in n-type silicon below insulator-to-metal transition

A L Danilyuk¹, S L Prischepa^{1,2,5} , A G Trafimenko¹, A K Fedotov^{3,4},
I A Svito⁴ and N I Kargin²

¹ Belarusian State University of Informatics and Radioelectronics, P. Browka 6, Minsk, 220013, Belarus

² National Research Nuclear University MEPhI, Kashirskoe Highway 31, Moscow, 115409, Russia

³ Institute for Nuclear Problems of Belarusian State University, Bobruiskaya 11, Minsk, 220006, Belarus

⁴ Belarusian State University, Nezavisimostci av. 4, Minsk, 220006, Belarus

E-mail: prischepa@bsuir.by

Received 9 October 2019, revised 20 January 2020

Accepted for publication 31 January 2020

Published 3 March 2020



CrossMark

Abstract

We report on the electric transport properties of Si heavily doped with Sb at concentration just below the insulator-to-metal transition in the temperature range 1.9–3.0 K for current density $J < 0.2 \text{ A cm}^{-2}$. The change in the sign of the temperature dependence of the differential resistivity \mathcal{R} was observed: the $d\mathcal{R}/dT$ is positive if $J < 0.045 \text{ A cm}^{-2}$ whereas it becomes negative at $J > 0.045 \text{ A cm}^{-2}$. The effect is explained assuming the exchange by electrons between the upper Hubbard band (UHB) and the conduction band. The obtained J dependencies of the activation energy, nonequilibrium concentration, mobility and scattering time of the conduction electrons correspond well to this hypothesis. The reason for charge instability is the Coulomb repulsion between electrons occupying states both in the UHB and conduction band. The estimated J dependencies of the conduction electrons lifetime and concentration of the D^- states in the UHB strongly supports this assumption.

Keywords: charge carrier instability, upper Hubbard band, delocalization, temperature coefficient of differential resistivity, correlated electron system

(Some figures may appear in colour only in the online journal)

1. Introduction

The physical mechanisms and effects associated with the manifestation of charge instability and an electronic Mott insulator-to-metal transition (IMT) in correlated electron systems are still the subject of intensive investigation [1–3]. The hallmark of the IMT is a change from the case of strong localization of charge carriers and the gap in the density of states (DOS) (insulating side of the IMT) to complete or partial delocalization and the disappearance of the gap (metallic side of the IMT). The reasons for this transition may be different and depend on the material and systems under investigation. Numerous studies are traditionally conducted on

silicon doped with elements such as Co [4], S [5, 6], Ti [7, 8], Se [9], Bi [10, 11] and V [12]. These works mainly address the issues of obtaining hyperdoped silicon and physics of IMT research in it related to the creation of the intermediate band in the band gap of silicon.

Observation of the Mott insulator state in underdoped high temperature superconductors (HTSC) and transition to the superconducting state in optimally doped HTSC [13] expanded the class of materials that are inherent in the IMT. Nowadays, it is reliably established that the IMT is a characteristic feature of a granular and homogeneously disordered superconducting thin films [14], networks of superconducting nanowires [15], vortex systems [16], quantum spin liquids [17], layered perovskite oxides [18]. Various relevant drives can be applied to induce the IMT. Among them, it is worth

⁵ Author to whom any correspondence should be addressed.

noting the level of doping, temperature, magnetic and electric fields, internal stresses in the crystal lattice, external injection of charge carriers.

Attention is paid, in addition to the IMT itself, to study of the related effects. These include, e.g. spin–orbit coupling induced by bismuth doping in silicon [11], variable-range hopping and Kondo effect signatures [12], conductivity and magnetoresistance near IMT [19], Coulomb gap in a doped semiconductor near IMT [20], spin relaxation near IMT and in hopping transport [21], hopping conductivity and IMT in doped semiconductor nanocrystal films [22, 23], emergence of metallic meta-stable phase [24] and metallic quantum fluctuations [17]. This indicates an interest also in the effects *close* to the IMT, the study of which will help to compliment and clarify microscopic nature of the insulator-to-metal transition.

Recently, the peculiarities of conductivity in non-compensated silicon doped with Sb (10^{18} cm^{-3}) have been investigated [25–28]. It was found that in the temperature (T) range of 28–90 K an activation mechanism with an energy of 1.73 meV occurs due to motion of electrons along the almost delocalized states. Then, in the range of 5–20 K, the spin-dependent Mott variable range hopping mechanism prevails, and at lower temperatures, 1.9–3 K, an activation conduction mechanism with an activation energy of 1.48 meV *returns*. The latter is caused by the existence of the lower and upper Hubbard bands (LHB and UHB, correspondingly) and is not suppressed by the magnetic field [28]. This low- T range of carrier transport is characterized by the charge instability and the negative differential resistance (NDR) region with increasing current density [27, 28]. Since the critical concentration for IMT in antimony-doped silicon is $(3 \pm 0.2) \times 10^{18} \text{ cm}^{-3}$ [29] and slightly increases only below 1 K [30, 31], it can be argued that the effects identified in [25–28] in Si:Sb precede the appearance of the IMT. Thus, further investigation of these properties is relevant for a more complete understanding of the carrier transport mechanisms manifested near the IMT in different temperature ranges.

On the other hand, charge instability and NDR are promising for applications. Indeed, investigation of charge carrier transport in Si and Si-based nanostructures is relevant for silicon nanoelectronics, quantum computing, non-volatile memory and logic with low power consumption and switching energy [32–34]. Significant progress has been achieved for a wide range of nanostructures, like atom devices based on single dopants in silicon nanostructures [35], spin transistors [36] and logic elements [37]. However, there are still many problems to be solved, both physical and technological. Those include, for example, reducing the power consumption when switching logic and memory elements, improving the parameters of MOSFET, increasing the selectivity of controlling qubits and the accuracy of electrical measurements of their state. Some of these problems can be solved by using non-linear effects in silicon, such as charge carrier instability, NDR and IMT [38].

In this work, by analyzing the current and temperature dependences of differential resistivity extracted from current–voltage characteristics (CVCs) $\mathcal{R}(J) = dE/dJ$ (E being the electric field and J being the density of current), various

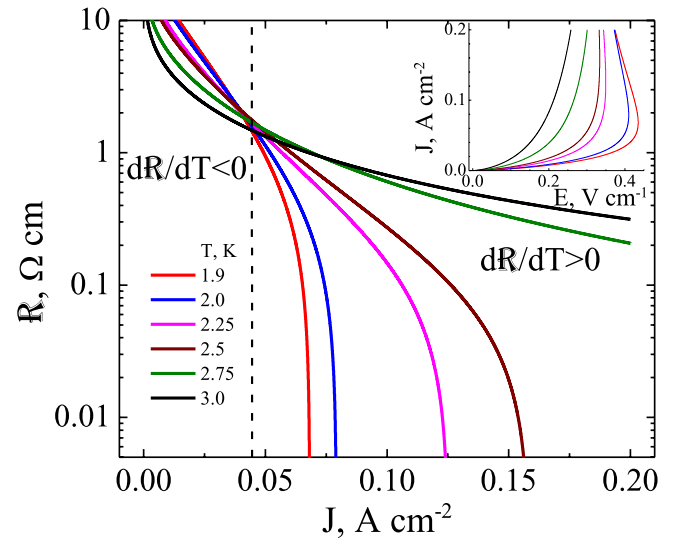


Figure 1. $\mathcal{R}(J)$ dependencies at different T . Vertical dashed line separates regions with negative (left) and positive (right) sign of the TCR. Inset: CVC at different T . The colors and temperature values on the inset correspond to those on the main panel.

electrophysical parameters were estimated that has allowed to discuss mechanisms of charge carrier instability occurrence and change of a sign of temperature coefficient of differential resistivity (TCR) in the region preceding the NDR in Si:Sb below the IMT, i.e. on the insulating side of this transition.

2. Experimental

Samples used in this work were doped with Sb (10^{18} cm^{-3}) single crystalline Si (100) grown by Czochralski method. Indium Ohmic contacts were used for transport and Hall effect measurements. Samples were inserted into the cryogen free measuring system (Cryogenic Ltd., London) with the superconducting magnet. More details about samples characterization and measurements can be found elsewhere [27, 28, 39].

The inset to figure 1 shows low- T CVCs demonstrating the charge carrier instabilities preceding the NDR regions [27]. It is seen that when T decreases, the region preceding the transition to the NDR regime approaches the electric field axes and stretches along it. In the region close to the onset of the NDR regime, the Hall measurements have been performed. They revealed that, at $J = 0.02 \text{ A cm}^{-2}$ and $T = 2 \text{ K}$ the concentration of the conduction electrons is $n = (6 \pm 0.75) \times 10^{16} \text{ cm}^{-3}$. This allowed us to estimate the values of mobility μ and conduction electrons scattering time τ (pulse relaxation time), which turned out to be equal $\mu \approx 15.4 \pm 2.3 \text{ cm}^2 \text{ V}^{-1} \cdot \text{s}^{-1}$ and $\tau \approx 2 \text{ fs}$.

On the base of the measured CVCs the differential resistivity \mathcal{R} at different J and T was obtained. For initial parts of CVCs ($J < 5 \text{ mA cm}^{-2}$, not shown) the \mathcal{R} values are in the range of 60–100 $\Omega \times \text{cm}$. The $\mathcal{R}(J)$ dependencies for the studied temperature range and $J > 5 \text{ mA cm}^{-2}$ are plotted in the main panel of figure 1. One of the remarkable features of these dependencies is the change of the TCR sign, from negative at low currents to positive at high ones.

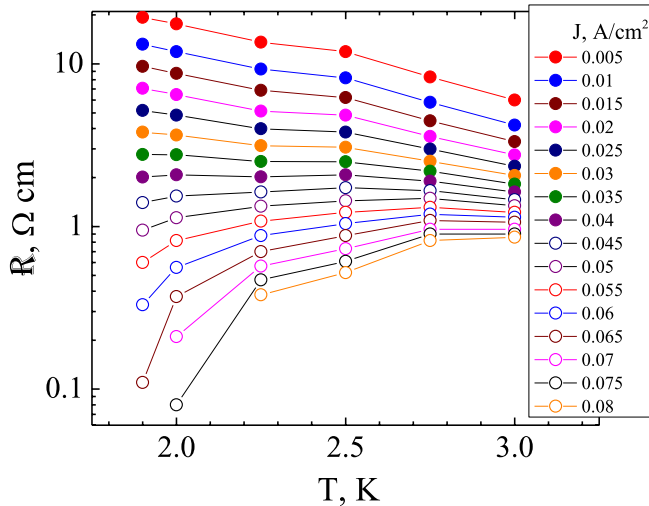


Figure 2. $\mathcal{R}(T)$ dependencies at different J .

This change is better seen in figure 2, where we plot the $\mathcal{R}(T)$ dependencies at different J . This result allows analyzing in detail the sign of the first derivative $d\mathcal{R}/dT$. As follows from this figure, at low J values, $\mathcal{R}(T)$ increases monotonically as the temperature decreases. Such a temperature behavior of resistance is characteristic of an insulator. However, above a value of $J \approx 40 \text{ mA cm}^{-2}$, the temperature dependence $\mathcal{R}(T)$ becomes non-monotonic: with decreasing temperature, the differential resistivity first increases (at $T > 2.5 \text{ K}$ and $40 \text{ mA cm}^{-2} < J < 70 \text{ mA cm}^{-2}$) and then starts to decrease (at $T < 2.5 \text{ K}$) for all $J > 40 \text{ mA cm}^{-2}$.

The differential resistivity at $J > 65 \text{ mA cm}^{-2}$ drops by almost one order of magnitude at low temperatures, showing a metallic-like behavior.

Similar change in the temperature dependence of the resistance was observed earlier on two dimensional (2D) very high quality silicon MOSFET samples with electron densities below 10^{11} cm^{-2} and electron mobility greater than $4 \times 10^4 \text{ cm}^2 \text{ V}^{-1} \text{ s}^{-1}$, when changing the degree of doping of the substrate [3, 40–43]. At such low electron densities, the Coulomb interaction becomes the main important parameter. With increasing the disorder in the substrates, however, the pure metallic behavior was never observed [44]. The same behavior with respect to the change in the sign of the TCR with the change of the substrate level doping is also characteristic of GaAs heterostructures [45–47] and SiGe/Si/SiGe quantum wells [48]. For these 2D systems such a crossover in the sign of the resistance versus temperature behavior at different level of doping is associated with the two-dimensional IMT [3, 44, 49, 50].

Samples studied in this work are essentially three dimensional (3D). Besides, the doping level of the samples remains constant, ensuring that they stay on the dielectric side of the IMT. What changes is the injected charge carrier concentration. Therefore, to find out the reason for the change in the TCR sign, it is necessary to conduct a detailed study of the transport and scattering mechanisms as a function of charge carrier concentration.

3. Discussion

3.1. Qualitative arguments

We believe that the discovered patterns are due to the manifestation of the following physical processes. As was shown earlier, the mechanism of current transport in the initial part of the CVCs is mainly of the activated-type due to the predominant capturing of the electrons by neutral impurity states D^0 in the LHB that transforms them into negatively charged D^- states [27, 28]. The dominance of this activation mechanism causes a negative sign of the TCR (insulating-like behavior). The increase in the current density is accompanied by a sharp decrease of \mathcal{R} (more than two orders of magnitude) and transition to a positive sign of the TCR (metal-like behavior). Such a TCR crossover indicates a likely change in the carrier transport mechanism, from the predominance of electron capture to the local D^0 states at $d\mathcal{R}/dT < 0$ to a purely transport by conduction band when the derivative $d\mathcal{R}/dT$ becomes positive. In this case, in contrast to the previous mechanism, in which the capture of electrons on the D^0 states prevails, the main contribution to the resistance is due to the scattering of injected nonequilibrium electrons in the conduction band.

The above hypothesis is supported by the fact that under the considered conditions, due to the freezing of the major charge carriers, the injected electrons firstly are intensely captured by the neutral D^0 states, their concentration in the conduction band is insignificant. The increase in the concentration of injected electrons leads to a sharp increase in current and instability [51, 52]. Therefore, the mechanism of the charge carrier instability in this case is associated with the effect of nonequilibrium concentration of conduction electrons on the electron exchange processes with the UHB. Achieving a certain nonequilibrium concentration of conduction electrons with increasing current density serves as a trigger of the process of D^- states delocalization due to the Coulomb interaction, which is accompanied by a sharp change in the shape of CVC and the transition to the NDR regime.

The proposed hypothesis reflects appearance of the UHB and its apparent overlap with the conduction band. This can be considered as a forerunner of the insulator-to-metal transition. Below we will try to elucidate the role of the D^- states and their interaction with the edge states of the conduction band in emergence of the charge carrier instability.

3.2. Quantitative analysis

3.2.1. Concentration instability and activation energy. To confirm the above qualitative arguments, a quantitative analysis of the experimental data was carried out. Close to the NDR region the \mathcal{R} value sharply decreases, therefore, the activation energy ε_a should also decrease. In this regard, we can apply a model of concentration instability in semiconductors [52]. It assumes that the increase of the concentration of conduction electrons causes decrease of the activation energy according to the relation

$$\varepsilon_a = \varepsilon_{a0} - (n/n_k)kT, \quad (1)$$

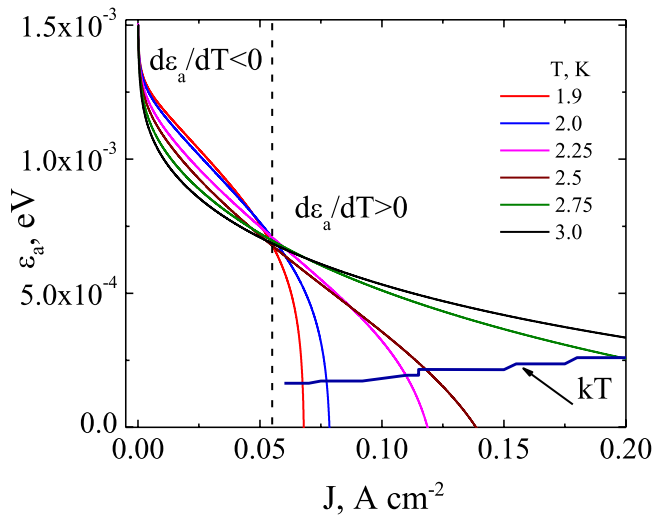


Figure 3. Dependence of the activation energy ε_a of the conduction electrons on the current density at different T . Vertical dashed line separates regions with negative (left) and positive (right) sign of the $d\varepsilon_a/dT$ dependencies. The restriction caused by the thermal energy kT is also shown.

where n_k is a model parameter, at which the energy ε_a decreases on kT , k is the Boltzmann constant. Based on the activation mechanism it is possible to obtain current dependencies of ε_a , see figure 3.

It follows from figure 3 that the character of the $\varepsilon_a(J)$ dependence differs for $J < 0.055 \text{ A cm}^{-2}$ and $J > 0.06 \text{ A cm}^{-2}$. A faster decrease in the activation energy with the current increase in the first region is observed at $T = 3 \text{ K}$, and in the second, at $T = 1.9 \text{ K}$. Thus, an analogue of the TCR crossover is observed in the $\varepsilon_a(J, T)$ dependences.

3.2.2. Concentration of conduction electrons n and D^- states n_t . According to the obtained estimations we deduce $n/n_k = 2.78 \pm 0.6$ at $J = 0.02 \text{ A cm}^{-2}$ and $T = 2 \text{ K}$. Based on the experimentally determined from Hall measurements n value we estimate $n_k = (2.5 \pm 0.45) \times 10^{16} \text{ cm}^{-3}$. Supposing that the characteristic concentration n_k is temperature independent, the nonequilibrium concentrations of the conduction electrons n at different J has been obtained. This result is shown in figure 4(a). As is seen, the values of n for small current densities J are temperature independent. But above $J \approx 0.02 \text{ A cm}^{-2}$ n becomes function of T , so that the observed sharp increase of concentration with the J increase depends on T . For higher temperatures the maximum in the concentration is shifted towards the largest J . The result of figure 4(a) confirms the hypothesis that the charge transport mechanism could change from the activation to the band one with increasing J .

Using the obtained $n(J)$ dependencies we performed the evaluation of the concentration of electrons n_t trapped by the D^0 states (i.e. the concentration of the D^- states). It can be obtained from the balance equation [53]

$$\frac{dn_t}{dt} = nR_n(N_d - n_t) - Gn_t, \quad (2)$$

where R_n is the capture rate, N_d is total concentration of donors, $G = G_0 \exp(-\varepsilon_a/kT)$ is a probability of electron generation

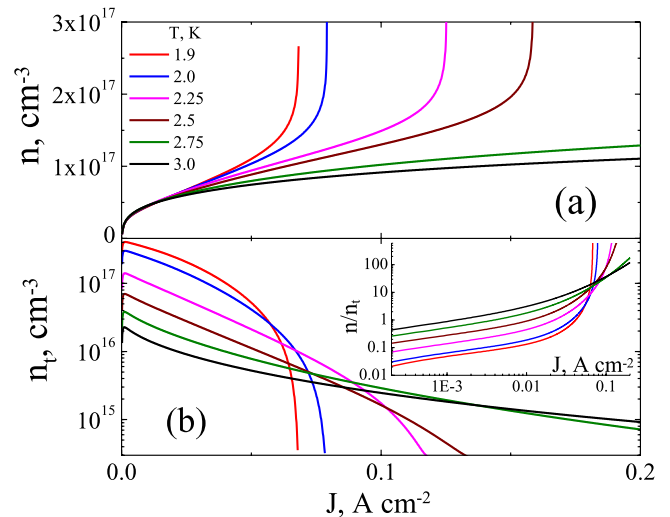


Figure 4. (a) Nonequilibrium concentration of the conduction electrons n versus J ; (b) Concentration of D^- states n_t versus J at different T . Inset: The relation n/n_t versus J at different temperatures. The colors and temperature values on the panel (b) and inset correspond to those on the panel (a).

from D^- states to the conduction band, G_0 is a frequency factor determined by the vibrational spectrum of the impurity centers. According to [54], for Sb in Si $G_0 = (2-3) \times 10^{13} \text{ Hz}$. Considering the balance equation (2) for the stationary state, $dn_t/dt = 0$, we get

$$n_t = nR_n N_d / (nR_n + G). \quad (3)$$

To estimate the capture rate on D^0 state we apply the model of the electron capture on the hydrogen-like neutral donor with the emission of the acoustic phonon [55]. Since the negatively charged D^- state exists only in a singlet state, in conditions when free carriers and impurity centers are not polarized, the capture can occur only in one quarter of the total number of the collision acts [55]. With this in mind, the rate of capture is determined by the expression [55]

$$R_n = \zeta^2 \frac{\pi^3}{16l_0} \left(\frac{2\varepsilon_a}{m_d} \right)^{\frac{1}{2}} \left(\frac{\hbar}{m_d s} \right)^3 \psi(\varepsilon_a), \quad (4)$$

where $\zeta = 1.1$ is a numerical coefficient, l_0 is the electron mean free path, \hbar is the reduced Plank constant, s is the sound speed in Si, m_d is the mass of the density of states and the wave function $\psi(\varepsilon_a)$ is expressed as

$$\psi(\varepsilon_a) = \frac{4}{\pi^2} \left(\tan^{-1} \left(\frac{1}{x} \right) + \frac{x}{x^2 + 1} \right)^2, \quad x = \frac{\sqrt{2m_d s^2 \varepsilon_a}}{\varepsilon_a + \varepsilon_n},$$

where ε_n is the thermal energy of the conduction electrons.

In figure 4(b) we show the obtained n_t versus J dependence. At low J the concentration of D^- states is maximum, which confirms the assumption of the predominance of the current transfer mechanism by capturing the injected electrons by the states in the UHB. If J increases, we observe the n_t decrease, which is mostly pronounced close to transition to the NDR regime. The effect of temperature is that at a lower T there is a higher concentration in the region of small currents and a sharper decrease in the concentration n_t with an increase

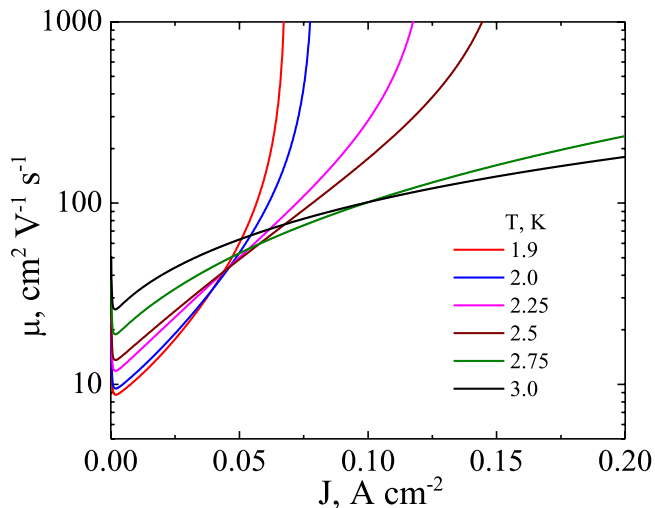


Figure 5. The electron mobility μ of the conduction electrons versus J at different T .

in current, turning into a smooth decrease with the temperature increase. This correlates with a decrease in the activation energy when current increases, presented in figure 3, and evidences that, with a decrease in temperature the delocalization of D^- states becomes more efficient since the concentration instability occurs at lower J .

The obtained $n_t(T)$ dependences clearly show that the current transfer correlates with the interrelated redistribution of electrons between the states in the conduction and upper Hubbard bands, the ratio between which varies with the current increase and transition to the NDR regime, see inset to figure 4(b).

3.2.3. The mobility μ , scattering time τ and lifetime τ_{lf} of conduction electrons. The obtained $\mathcal{R}(J)$, $n(J)$ and $n_t(J)$ dependencies allow evaluating the $\mu(J)$, $\tau(J)$ and lifetime of conduction electrons $\tau_{lf}(J)$ dependencies.

In figure 5 we show the obtained electron mobility versus J at different temperatures. It follows that μ increases with J despite the increase of n . This is due to a sharper drop in \mathcal{R} with J compared to an increase in n with J increase. This is seen better for $T = 1.9\text{K}$ at which a sharp increase of μ is observed at lower J with respect to higher temperatures. Note that the electron mobility values hugely increase by 2 orders of magnitude at constant temperature (1.9K and 2.0K) within a narrow range of current density. To obtain such a variation of the mobility in typical n -doped semiconductors, like, e.g. Si-doped (Al,Ga)As, a variation of temperature over a few hundreds of degrees should be realized [56–58]. This issue will be discussed later.

In figure 6(a) the results of electron scattering time τ versus J are present. It follows that τ is about 1.5–5 fs for $J = 0.02\text{ A cm}^{-2}$ depending on T and increases up to 0.1–1 ps with the current growth. This variation of τ indicates the change in the scattering mechanism when approaching the NDR regime.

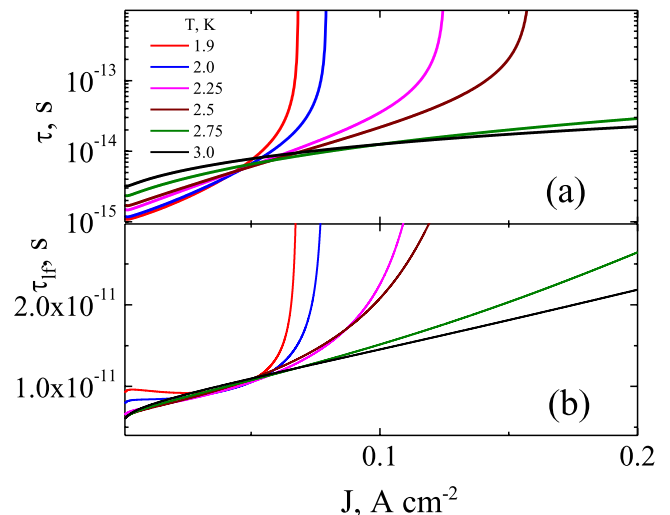


Figure 6. Scattering time τ and lifetime τ_{lf} of conduction electrons versus J at different T . The colors and temperature values on the panel (b) correspond to those on the panel (a).

The lifetime relative to capture to the D^0 states with the concentration $N_{D0} = N_d - n_t$ is determined from the known expression $\tau_{lf} = 1/(R_n N_{D0})$ [53]. Substituting equation (3) into the above expression for τ_{lf} we get

$$\tau_{lf} = \frac{1}{R_n N_d} \left(1 + \frac{n R_n}{G} \right). \quad (5)$$

The results of the calculations of τ_{lf} are shown in figure 6(b). Parameters of the model of electron capture by neutral centers in Si were taken as $\varepsilon_n = (0.214-0.27)\text{ meV}$, $m_d = 0.33m_0$, $s = 9.15 \cdot 10^5\text{ cm s}^{-1}$, $l_0 = 7.5 \cdot 10^{-4}\text{ cm}$ [55]. As follows from figure 6(b), the electron lifetime weakly depends on J and T up till a certain $J \approx 0.055\text{ A cm}^{-2}$, beyond which τ_{lf} increases by several times, which corresponds to the decrease of the capture rate on the states in the UHB.

From the $n(J)$, $n_t(J)$ and $\tau(J)$, $\tau_{lf}(J)$ results it is possible to plot the behavior of τ and τ_{lf} as a function of both carrier concentration n and concentration of D^- states n_t at different temperatures. This result is shown in figures 7(a) and (b), respectively. It follows from figure 7(a) that, up till a certain value of n , approximately equal to n_k , the scattering time varies slightly indicating that the scattering mechanism is unchanged. At $n > n_k$ we observe the significant increase of τ . From that it follows that the transition to a different scattering mechanism is due to the reduction of the contribution of the mechanism prevailing at $n < n_k$. The latter is confirmed by the obtained regularity of τ increase with the decrease in the concentration n_t , figure 7(b). Therefore, we may consider the parameter n_k introduced in the model of the concentration instability of section 3.2.1, as a critical concentration, at which the scattering mechanism changes.

The obtained $\tau_{lf}(n)$ dependence suggests that for $n < n_k$ when $\tau_{lf} < 10\text{ ps}$ and varies insignificantly, the mechanism of the charge transfer on the localized states prevails. For $n > n_k$ the observed increase of the lifetime is most likely associated

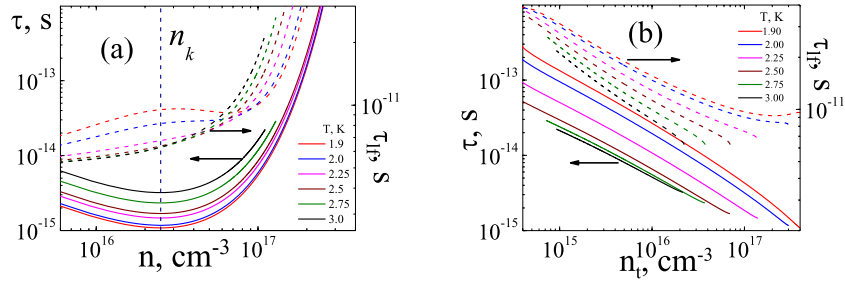


Figure 7. Scattering time τ (left axes solid lines) and lifetime τ_{lf} (right axes, dashed lines) of conduction electrons versus (a) their concentration n and (b) concentration of D^- states n_t . Vertical dashed line in panel (a) corresponds to the n_k value evaluated in section 3.2.1.

with the change of the mechanism of the charge transfer from localized states to the band conduction mechanism. This is also confirmed by an increase in the lifetime with a decrease in the n_t concentration, figure 7(b).

3.2.4. Model estimation of the scattering time τ . To identify the prevailing mechanism of electron scattering, a model estimation of τ was carried out. In the low T region, the main mechanism is the scattering of conduction electrons by neutral and charged impurities, whereas the scattering by phonons does not give a significant contribution. The estimations using the known Erginsoy and Brooks-Herring [59] models in the region of small J (not greater than 0.05 A cm^{-2}) revealed a significant discrepancy with the experimental data.

The analysis showed that in this case the conduction electrons possess by low energy (characteristic thermal energy is $\varepsilon_n < 0.3 \text{ meV}$), and the localized electrons due to the low binding energy of the D^- states are characterized by a relatively large effective Bohr radius of 8.5 nm. In this regard, we assumed the process of scattering of conduction electrons on D^- states by the mechanism of electron–electron scattering. The specificity of such a mechanism is that the conduction electrons are thermalized, and the electrons of the D^- states are bound. Considering this, the model of electron–electron scattering in the collision of an electron with a stationary target [59] was chosen with numerical correction [60]

$$\frac{1}{\tau} = \frac{nq^4 L(\beta, \varepsilon_n)}{4 \times 2^{3/2} \pi \kappa^2 m_n^2 \varepsilon_n^{3/2}} \quad (6)$$

where q is the electron charge, m_n is the effective mass of the conduction electron, β is the inverse screening length, L is a function of β and ε_n , which in view of complexity is not given explicitly here. It was obtained that the scattering time is $\tau = 1\text{--}3 \text{ fs}$, which is in good agreement with the experimental values. When J increases, the τ increases, that corresponds to the drop in the concentration of D^- states. For $J > 0.05 \text{ A cm}^{-2}$, when the scattering time is increased up to 60–100 fs, the change of scattering mechanism occurs: the scattering by neutral states becomes predominant.

3.2.5. Energy diagrams and parameters of the Hubbard model. The obtained current and temperature dependencies of ε_a , n , μ , τ and τ_{lf} point to the fact that the most likely mechanism of concentration instability is the Coulomb repulsion (CR) between electrons occupying the D^- states and the

conduction band. Due to this, a fluctuating potential relief arises, in UHB and conduction band both. As a result, UHB and the conduction band are overlapped in agreement with the model of concentration instability in semiconductors. Below we consider the possible reasons for this broadening.

The energy structure of the UHB is determined by the fact that the D^- states are charged and interact electrostatically both with each other and with conduction electrons. Also, in this case, the fluctuating potential in the UHB is affected by conduction electrons, since they are in a small electric field (not more than 1 V cm^{-1}) and possess of a relatively low thermal energy (0.214–0.27 meV). In addition, the system under consideration is characterized by a high concentration of charge carrier scattering centers, i.e. D^- and D^0 states, which contributes to the increased randomization.

To support above physical picture, we determine parameters of the Hubbard model which describes our samples. Actually, there are two main parameters: the matrix elements of hopping t and the electron–electron repulsion U . The bandwidth $W = 2zt$ is often considered instead of t . Here z is the number of the nearest neighbors. One of the approaches to determine the parameters W and U for correlated electron system is the adopted local density approximation (LDA) of the density functional theory—LDA + U [61–63]. In this approach, the CR leads to the appearance of the LHB and UHB separated by the energy U . However, in our case, there is no need to use LDA + U approximation, since the LHB does not change (i.e. the electrons of the D^0 states are frozen and the doping impurities are not ionized). In this case, we will only consider the filling of the UHB, i.e. the appearance of D^- states. The value of U is found within the LDA taking into account the exchange–correlation contribution to the energy [64–66].

For the case of small J , when $n_t > n$ (figure 4), the electrons are concentrated mainly in the UHB, so that the total energy of the electron system, referred to a single electron, can be written as

$$\varepsilon_{tot}(n_t) = t_S(n_t) + U_A + U_H(n_t) - \varepsilon_{ex}(n_t) - \varepsilon_c(n_t), \quad (7)$$

where the first term is for kinetic energy, U_A is the short-range potential for the electron–neutral atom interaction, U_H is the Hartree term for direct Coulomb interaction, ε_{ex} and ε_c correspond to the exchange–correlation. For the case when the temperature of an electron system is below the Fermi one, the following expressions for contributions to the energy (7) can be applied [65]:

$$t_S(n_t) = (3/10) (\hbar^2/m_e) (3\pi^2 n_t)^{2/3}, \quad (8)$$

$$U_H = \xi q^2 / [4\pi\kappa r_S(n_t)], \quad (9)$$

$$\varepsilon_{ex}(n_t) = q^2 / [4\pi\kappa] \cdot (3/4\pi) \cdot (3n_t\pi^2)^{1/3}, \quad (10)$$

where ξ is a lattice sum that depends on the type of arrangement of neighbor electrons, $r_S(n_t) = (3/4\pi n_t)^{1/3}$ is the average distance between electrons, κ is the absolute permittivity of silicon, q is the elementary charge. To take into account the contribution of the correlation energy, we use the Hedin and Lundqvist approximation [67], which is valid for $r_S/a_B > 1$ (a_B being the Bohr radius),

$$\varepsilon_c(n_t) = q^2 / [4\pi\kappa] \cdot (1/2a_B) C[(1+y^3) \ln(1+y^{-1}) + y/2 - y^2 - 1/3], \quad (11)$$

where $y = r_S/21a_B$, $C = 0.045$.

Calculations of the parameters $U = U_H(n_t) - \varepsilon_{ex}(n_t) - \varepsilon_c(n_t)$ and $W \approx t_S(n_t)$ revealed that, for the case $n_t = 10^{16} - 4 \times 10^{17} \text{ cm}^{-3}$, i.e. $n_t > n$, they are $U = 2.25 - 10 \text{ meV}$ and $W = 0.5 - 3.2 \text{ meV}$. Therefore, the ratio U/W is in the range of 4.5–3.1, indicating that the correlated electron system is similar to the Mott insulator [68, 69]. The Mott insulator—like behavior in our case is associated with the presence of fluctuations of potential in the UHB. They promote charge transfer with the activation energy ε_a , which corresponds to the evaluated Hubbard parameters. In other words, the value of $\varepsilon_a = 1.48 \text{ meV}$ [28] could be interpreted as the energy of Coulomb fluctuations in the UHB.

The energy diagram for the case of *low current* density, when the localization of electrons in the UHB prevails, is shown schematically in figure 8(a). When creating it, we took into account the fact that the LHB is fully occupied (the impurity electrons are frozen) and the UHB is filled by trapping the injected conduction electrons. The LHB is separated from the conduction band by the ionization energy of Sb, $E_d = 43 \text{ meV}$ [70]. The UHB is higher in energy from the LHB by U and the charge transfer through the UHB occurs by an activation mechanism with the energy of 1.48 meV due to fluctuations of the Coulomb potential.

For the case of a *higher current* densities, when the concentration of conduction electrons is significantly greater than in the UHB, i.e. $n \gg n_t$ (figure 4), to evaluate the parameters of the Hubbard model the influence of the conduction electrons should be taken into account. In this case, conduction electrons, which are characterized by relatively low kinetic energy, will be concentrated near the bottom of the conduction band, causing random fluctuations of the bottom of the conduction band E_c . Due to such fluctuations, the conduction band expands and overlaps with the UHB. This factor can be taken into account when applying the fluctuation model [71], in which the magnitude of such an expansion is defined as

$$W' = [q^2/\kappa] \cdot (\lambda_{TF} n / 4\pi)^{1/2}, \quad (12)$$

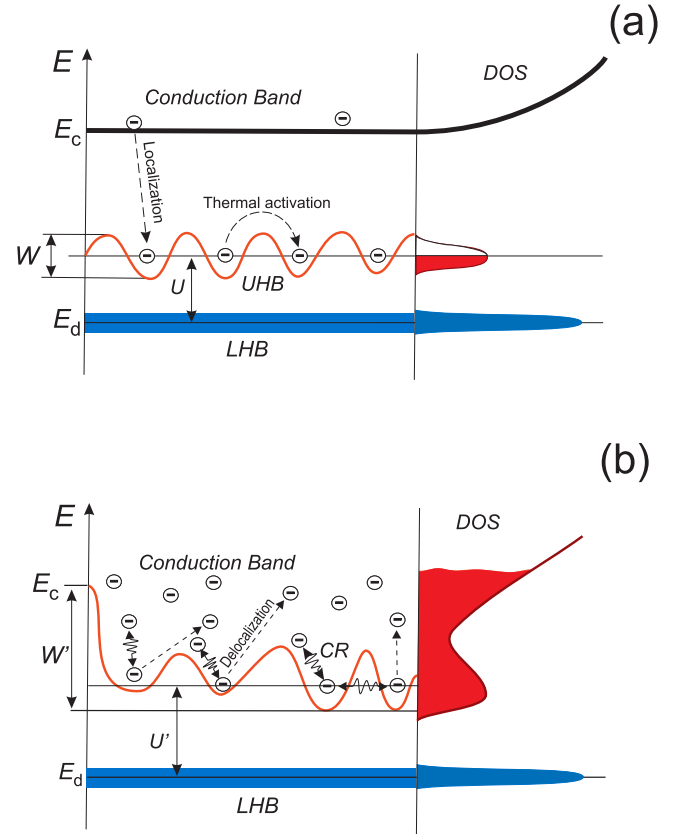


Figure 8. Schematic representation of the energy diagram for the case of low (a) and higher (b) current densities. For details see the text.

where λ_{TF} is the Thomas–Fermi screening length, $\varepsilon_F = (\hbar^2/2qm_e) \cdot (3\pi^2 n/M)^{2/3}$ is the Fermi energy for the system of electrons of concentration n at temperature smaller than the Fermi temperature, $M = 6$ is the number of equivalent minima in the silicon conduction band.

The performed estimations revealed that, $W' = 17 - 30 \text{ meV}$ for $n = (1 - 3) \times 10^{17} \text{ cm}^{-3}$. According to the equations (8)–(11), the U' values are in the range of 5–10 meV. Thus, the ratio $U'/W' \approx 0.3$. This estimation gives the upper limit, since it does not take into account that conduction electrons can be transferred by conduction band with greater energy. However, given the nature of the system under consideration, in which the external electric field is very small, the charge transfer will occur at the bottom of the conduction band and the above estimation of the parameter W' can be accepted as relevant.

The energy diagram for *higher current* densities is shown in figure 8(b) considering that the Coulomb interaction between electrons in the conduction band and in the UHB leads to the delocalization of the latter and a decrease of the D^- states concentration. As a result, upon potential fluctuations caused by randomly distributed charges, there is a broadening and overlap of the conduction and D^- bands.

At the microscopic level, the overlap of these bands could be described by the following mechanism. Electron of the D^- state has a final binding energy ε_a . In a set of randomly

arranged D^- states there will also be pairs whose Coulomb interaction energy exceeds ε_a . One of the electrons in such pairs leaves its neutral donor and is localized at some potential minimum of the conduction band edge (figure 8(b)). In other words, due to the Coulomb repulsion between D^- states and conduction electrons, the latter will ‘push out’ the electrons from the D^- states, or rather, do not allow the conduction electrons to be localized at the D^0 states. Considering only pairwise interaction, the concentration of such ‘pushed out’ electrons n_{tc} can be estimated from the expression $n_{tc} = \int_{\varepsilon_a}^{\infty} g(\varepsilon) d\varepsilon$, where $g(\varepsilon)$ is the DOS of D^- electrons that are affected by the Coulomb interaction ε with neighbors [72]. For the considered system we determined that $g(\varepsilon) = 4\pi\xi_n n_t (n_t + n)r^2 (dr/d\varepsilon)$, $\varepsilon = (2q/\kappa r) \exp(-\beta r)$, where ξ_n is a coefficient introduced to account for the ratio between the number of electrons in D^- states and conduction electrons, $\xi_n = 1 - (1/2)/\{1 + \exp[(n - n_t)/n_{t0}]\}$. Here n_{t0} is the broadening parameter of the transition from $n < n_t$ to $n > n_t$. At $n < n_t$, $\xi_n = 1/2$, whereas at $n > n_t$, $\xi_n \rightarrow 1$.

The obtained estimations of the n_{tc}/n_t variation with n at $T = 1.9$ K revealed that its value is within the limit of 15%–20% for $J < 0.06$ A cm $^{-2}$, and it significantly increases up to almost 100% for $J = 0.06$ – 0.08 A cm $^{-2}$. Similar dependencies have been obtained for the temperature range 2–2.5 K.

3.2.6. Huge increase of the electron mobility μ with J at constant temperature. In this section we turn back to the results of figure 3. It follows that μ increases two orders of magnitude, from 10 to 1000 cm 2 V $^{-1}$ s $^{-1}$ with current at a fixed temperature. It should be noted that as the current increases, the concentration of electrons in the conduction band n also increases, figure 4. It was obtained also that the μ and τ increase with decreasing of n_t , figures 3 and 7, respectively. It relates to the delocalization and change of the scattering mechanism. As shown above, the dominant mechanism at low currents (large n_t) is the electron–electron scattering at charged D^- states, and at high currents (small n_t)—scattering at neutral D^0 states. The latter is characterized by a significant increase in τ in comparison with the scattering on D^- states, figure 7.

Now we will consider the possible reasons for this effect. At small currents the dominant process is the localization of the injected electrons at the D^0 states. This restricts significantly the electron mobility, because the charge transfer occurs at the UHB with the activation energy $\varepsilon_a = 1.48$ meV and the reverse thermal emission of electrons from the D^- states to the conduction band is limited. In this case, the electron scattering time, which determines the conductivity, is 2–4 fs, and their lifetime is less than 10 ps, figure 7. These factors significantly restrict the mobility.

With the J increase, as shown above, the delocalization of the D^- states occurs due to the convergence of the conduction and upper Hubbard bands with increasing n . In this case both the scattering time and the lifetime are significantly increased, up to 0.1–1 ps and 30 ps, correspondingly, figure 7. This is because: (i) the charge transfer band expands: now the charge is carried out not in a narrow UHB (where $U/W > 1$), but in

a relatively wide energy range, where $W > U$, figure 8(b). Therefore, the CR does not restrict the charge transfer; (ii) the scattering mechanism changes: due to a decrease in the concentration of the D^- states scattering by neutral D^0 states becomes dominant. It is characterized by a significantly smaller influence on the change of the electron momentum compared to the charged D^- states. The attenuation of scattering at the D^- states, as well as the absence of ionized D^+ states due to freezing, leads to a significant increase in the electron mobility.

The increase in μ is also facilitated by an increase in the lifetime due to the restriction of the localization of injected electrons, as well as a drop in the binding energy ε_a of electrons at the D^- states, figure 3. Note, that with a decrease in the binding energy of electrons at the D^- states, the mobility increases significantly when scattering at neutral D^0 states [73].

The obtained effect of huge increase of the mobility is not typical for bulk semiconductors. For them, as is known, a change in the mobility for orders of magnitude requires the same change in temperature [56–58]. This is valid for Si at relatively small impurity concentrations (10^{14} – 10^{16} cm $^{-3}$). At an impurity concentration of 10^{17} – 10^{18} cm $^{-3}$, the mobility with temperature generally changes non-linearly—there is a characteristic maximum in the region of 150–200 K [74]. Since in our case the μ increases with the increase in the concentration of conduction electrons (due to a decrease in the concentration of localized n_t states), the analog of this effect is the mobility regularities in the inversion layers of n -MOSFET. In such structures at a fixed temperature, when the concentration of charge carriers varies, the mobility can vary widely [75–77]. In this case the mobility is determined by the density of the induced charge carriers in the inversion channel and the ability to regulate the scattering mechanisms, in particular, to exclude the dominance of scattering on charged states.

4. Conclusions

Low temperature transport properties of antimony doped silicon at concentration just below the insulator-to-metal transition have been performed. The charge carrier instability induced by the applied current has been observed. By studying the current dependences of electrophysical parameters, such as differential resistance, activation energy, concentrations of conduction electrons and of D^- states, electron mobility, scattering time, electron lifetime, we have shown that the resulting charge instability is due to delocalization of the electron states in the UHB caused by the Coulomb interaction with conduction electrons. Parameters of the Hubbard model describing the 3D system under consideration have been estimated. They revealed that, at small current densities, $J \leq 0.04$ A cm $^{-2}$, when activation carrier transport via the UHB occurs, $U/W \approx 3.1$ – 4.5 and we deal with the correlated electron system. The energy of the activated motion of electrons in this case can be considered as the energy of the Coulomb fluctuations in the UHB. At higher current densities, $J > 0.05$ A cm $^{-2}$, $U/W \approx 0.3$, delocalization of

the electrons in the UHB takes place resulting in overlap of conduction and upper Hubbard bands, so that the resistance drops significantly. In addition, we have demonstrated that the huge increase of the electron mobility is a significant feature of transition to the carrier transport by the delocalized band while keeping temperature constant. The main reason of the observed effects at impurity concentration below IMT is the charge instability controlled by current. The results obtained are useful for identifying the role of the UHB in the return of the activation conduction mechanism and the appearance of charge instability in such heavily doped silicon within the temperature range of 1.9–3 K. They are also promising for creation of novel energy-efficient logic elements, based on Si nanostructures.

Acknowledgments

SL Prischepa acknowledges the partial financial support of the ‘Improving of the Competitiveness’ Program of the National Research Nuclear University MEPhI—Moscow Engineering Physics Institute.

ORCID iDs

S L Prischepa  <https://orcid.org/0000-0001-9584-1926>

References

- [1] Shaw M P, Mitin V V, Schöll E and Grubin H L 1992 *The Physics of Instabilities in Solid State Electron Devices* (Berlin: Springer)
- [2] Mott N and Kaveh M 1983 *Phil. Mag.* B **47** 577
- [3] Dobrosavljević V, Trivedi N and Valles J M Jr 2012 *Conductor-Insulator Quantum Phase Transitions* (Oxford: Oxford University Press) p 566
- [4] Zhou Y, Liu F and Song X 2013 *J. Appl. Phys.* **113** 103702
- [5] Zhao Z-Y and Yang P-Z 2014 *Phys. Chem. Chem. Phys.* **16** 17499
- [6] Winkler M, Recht D, Sher M-Y, Said A, Mazur E and Aziz M 2011 *Phys. Rev. Lett.* **106** 178701
- [7] Liu F et al 2018 *Sci. Rep.* **8** 4164
- [8] Zhou Y, Liu F, Zhu M, Song X and Zhang P 2013 *Appl. Phys. Lett.* **102** 222106
- [9] Ertekin E, Winkler M, Recht D, Said A, Aziz M, Buonassisi T and Grossman J 2012 *Phys. Rev. Lett.* **108** 026401
- [10] Abramof E, Ferreira da Silva A, Sernelius B, de Souza J and Boudinov H 1997 *J. Mater. Res.* **12** 641
- [11] Rortais F, Lee S, Ohshima R, Dushenko S, Ando Y and Shiraishi M 2018 *Appl. Phys. Lett.* **113** 122408
- [12] García-Hemme E, Montero D, García-Hernansanz R, Olea J, Mártel I and González-Díaz G 2016 *J. Phys. D: Appl. Phys.* **49** 275103
- [13] Keimer B, Kivelson S A, Norman M R, Uchida S and Zaanen J 2015 *Nature* **518** 179
- [14] Baturina T I and Vinokur V M 2013 *Ann. Phys., NY* **331** 236
- [15] Salvato M, Cirillo C, Fittipaldi R, Prischepa S L, Vecchione A, De Nicola F, Castrucci P, De Crescenzi M, Scarselli M and Attanasio C 2016 *Carbon* **105** 544
- [16] Poccia N, Baturina T I, Coneri F, Molenaar C G, Wang X R, Bianconi G, Brinkman A, Hilgenkamp H, Golubov A A and Vinokur V V 2015 *Science* **349** 1202
- [17] Pustogow A et al 2018 *Nat. Mater.* **17** 773
- [18] Sow C, Yonezawa S, Kitamura S, Oka T, Kuroki K, Nakamura F and Maeno Y 2017 *Science* **358** 1084
- [19] Dai P, Zhang Y and Sarachik M 1992 *Phys. Rev. B* **45** 3984
- [20] Lee M, Massey J, Nguyen V and Shklovskii B 1999 *Phys. Rev. B* **60** 1582
- [21] Shklovskii B 2006 *Phys. Rev. B* **73** 193201
- [22] Chen T, Reich K, Kramer N, Fu H, Kortshagen U and Shklovskii B 2016 *Nat. Mater.* **15** 299
- [23] Fu H, Reich K and Shklovskii B 2016 *Phys. Rev. B* **93** 125430
- [24] Cirillo C, Granata V, Avallone G, Fittipaldi R, Attanasio C, Avella A and Vecchione A 2019 *Phys. Rev. B* **100** 235142
- [25] Fedotov A, Prischepa S, Danilyuk A, Svito I and Zukowski P 2014 *Acta Phys. Pol. A* **125** 1271
- [26] Fedotov A, Svito I, Fedotova V, Trafimenko A, Danilyuk A and Prischepa S 2015 *Semiconductors* **49** 705
- [27] Danilyuk A L, Trafimenko A G, Svito I A, Fedotov A K and Prischepa S L 2016 *Appl. Phys. Lett.* **109** 222104
- [28] Danilyuk A L, Trafimenko A G, Fedotov A K, Svito I A and Prischepa S L 2017 *Adv. Condens. Matter Phys.* **2017** 5038462
- [29] Castner T, Lee N, Cieloszyk G and Salinger G 1975 *Phys. Rev. Lett.* **34** 1627
- [30] Long A and Peppert M 1984 *J. Phys. C: Solid State Phys.* **17** L425
- [31] Finlayson D, Mason P and Tunstall D 1990 *J. Phys.: Condens. Matter* **2** 6735
- [32] Oda S and Ferry D (ed) 2005 *Silicon Nanoelectronics* (Boca Raton, FL: CRC Press)
- [33] Wolf S, Awschalom D, Buhrman R, Daughton J, von Molnár S, Roukes M, Chtchelkanova A and Treger D 2001 *Science* **294** 1488
- [34] Jansen R 2012 *Nat. Mater.* **11** 400
- [35] Moraru D, Udhiarto A, Anwar M, Nowak R, Jablonski R, Hamid E, Tarido J, Mizuno T and Tabe M 2011 *Nanoscale Res. Lett.* **6** 479
- [36] Huang B, Monsma D and Appelbaum I 2007 *Appl. Phys. Lett.* **91** 072501
- [37] Dery H, Dalal P, Cywiński Ł and Sham L 2007 *Nature* **447** 573
- [38] Wang S, Pan A, Chui C and Gupta P 2017 *IEEE Trans. Electron Devices* **64** 121
- [39] Fedotov A K, Prischepa S L, Svito I A, Redko S V, Saad A, Mazanik A V, Dolgiy A L, Fedotova V V, Zukowski P and Koltunovicz T N 2016 *J. Alloys Compd.* **657** 21
- [40] Kravchenko S V, Kravchenko G V, Furneaux J E, Pudalov V M and D’Iorio M 1994 *Phys. Rev. B* **50** 8039
- [41] Kravchenko S V, Mason W E, Bowker G E, Furneaux J E, Pudalov V M and D’Iorio M 1995 *Phys. Rev. B* **51** 7038
- [42] Kravchenko S V, Simonian D, Sarachik M P, Mason W and Furneaux J E 1996 *Phys. Rev. Lett.* **77** 4938
- [43] Pudalov V M, Brunthaler G, Prinz A and Bauer G 1998 *Physica E* **3** 79
- [44] Kravchenko S V and Sarachik M P 2004 *Rep. Prog. Phys.* **67** 1
- [45] Hanein Y, Meirav U, Shahar D, Li C C, Tsui D C and Shtrikman H 1998 *Phys. Rev. Lett.* **80** 1288
- [46] Lilly M P, Reno J L, Simmons J A, Spielman I B, Eisenstein J P, Pfeiffer L N, West K W, Hwang E H and Das Sarma S 2003 *Phys. Rev. Lett.* **90** 056806
- [47] Gao X P A, Boebinger G S, Mills A P, Ramirez A P, Pfeiffer L N and West K W 2005 *Phys. Rev. Lett.* **94** 086402
- [48] Melnikov M Y, Shashkin A A, Dolgoplov V T, Zhu A Y X, Kravchenko S V, Huang S-H and Liu C W 2019 *Phys. Rev. B* **99** 081106
- [49] Radonjić M M, Tanasković D, Dobrosavljević V, Haule K and Kotliar G 2012 *Phys. Rev. B* **85** 085133
- [50] Shashkin A A and Kravchenko S V 2019 *Appl. Sci.* **9** 1169
- [51] Lampert M A and Mark P 1970 *Current Injection in Solids* (New York: Academic)

- [52] Sandomirskii V, Sushanov A and Zdan A 1970 *Sov. Phys.–JETP* **31** 902
- [53] Sze S M 1981 *Physics of Semiconductor Devices* 2nd edn (New York: Wiley)
- [54] Pajot B, Kauppinen J and Antilla R 1979 *Solid State Commun.* **31** 759
- [55] Abakumov V N, Perel V I and Yassievich I N 1991 Nonradiative recombination in semiconductors *Modern Problems in Condensed Matter Sciences* vol 33, ed V M Agranovich and A A Maradudin (Amsterdam: North-Holland)
- [56] Ishikawa T, Saito J, Sasa S and Hiyamizu S 1982 *Japan. J. Appl. Phys.* **21** L675
- [57] Chand N, Henderson T, Klem J, Ted Masselnik W, Fischer R, Chang Y-C and Morkoc H 1984 *Phys. Rev. B* **30** 4481
- [58] Simserides C D and Triberis G P 1995 *J. Phys.: Condens. Matter* **7** 6317
- [59] Ridley B K 1982 *Quantum Processes in Semiconductors* (Oxford: Clarendon)
- [60] Abrahams E 1954 *Phys. Rev.* **95** 839
- [61] Cococcioni M and De Gironcoli S 2005 *Phys. Rev. B* **71** 035105
- [62] Anisimov V I, Aryasetiawan F and Lichtenstein A I 1997 *J. Phys.: Condens. Matter* **9** 767
- [63] Agapito L A, Curtarolo S and Nardelli M B 2015 *Phys. Rev. X* **5** 011006
- [64] Kohn W and Sham L J 1965 *Phys. Rev.* **140** A1133
- [65] Tkharev E and Danilyuk A 1985 *Vacuum* **35** 183
- [66] Jones R O and Gunnarsson O 1989 *Rev. Mod. Phys.* **61** 689
- [67] Hedin L and Lundqvist B I 1971 *J. Phys. C: Solid State Phys.* **4** 2064
- [68] Mott N F 1961 *Phil. Mag.* **6** 287
- [69] Brandow B H 1977 *Adv. Phys.* **26** 651
- [70] Pica G et al 2014 *Phys. Rev. B* **90** 195204
- [71] Kane E O 1985 *Solid-State Electron.* **28** 3
- [72] Petrov P V, Ivanov Yu L and Averkiev N S 2015 *Low Temp. Phys.* **41** 90
- [73] MacGill N C and Baron R 1975 *Phys. Rev. B* **11** 5208
- [74] Li S S and Thurber W R 1977 *Solid-State Electron.* **20** 609
- [75] Ho H-S, Chang I Y-K and Lee J Y-M 2007 *Appl. Phys. Lett.* **91** 173510
- [76] Chain K, Huang J-H, Duster J, Ko P K and Hu C 1997 *Semicond. Sci. Technol.* **12** 355
- [77] Masaki K, Taniguchi K and Hamaguchi C 1992 *Semicond. Sci. Technol.* **7** B573